Research Square

Preprints are preliminary reports that have not undergone peer review.
They should not be considered conclusive, used to inform clinical practice,
or referenced by the media as validated information.

Threshold Voltage Control and Normally-Off Operation in Diamond Two-Dimensional Hole Gas FETs Using Dielectric Interface Dipoles

Aditya Das Utsha
The University of Texas at San Antonio
Maitreya Dutta
maitreya.dutta@utsa.edu

The University of Texas at San Antonio

Article

Keywords: Aluminum oxide, Diamond, Hafnium oxide, High-k dielectric materials, Lanthanum oxide

Posted Date: November 13th, 2026

DOI: https://doi.org/10.21203/rs.3.rs-11546300/v1

License: This work is licensed under a Creative Commons Attribution 4.0 International License.
Read Full License

Additional Declarations: No competing interests reported.

Threshold Voltage Control and Normally-Off Operation in Diamond Two-Dimensional Hole Gas FETs Using Dielectric Interface Dipoles

Aditya D. Utsha[1] and Maitreya Dutta[1*]

[1]Department of Electrical Engineering, The University of Texas at San Antonio, One UTSA Circle, San Antonio, 78249, Texas, United States.

*Corresponding author(s). E-mail(s): maitreya.dutta@utsa.edu;
Contributing authors: adityadas.utsha@utsa.edu;

Abstract

Diamond two-dimensional hole gas(2DHG) field effect transistors(FETs) are normally-on devices. Prior methods to achieve normally-off operation like oxygen(O) termination and nitrogen(N) implantation modify the channel. For O-termination the sheet resistance increases by 1–2 orders of magnitude, whereas N-implantation results in loss of 70–98 % of on-current(I_{on}). In the present work, we demonstrate through a TCAD simulation study, how dielectric interface dipoles can be used to modulate threshold voltage(V_t) and achieve normally-off operation without affecting the channel. These dipoles are formed due to the difference in oxygen areal density which introduces a potential step whose sign depends on the deposition order. We study two pairs of dielectrics, Al_2O_3/HfO_2 and Al_2O_3/La_2O_3 which shift V_t by 0.84 V and 1.79 V respectively. The shift is independent of interface charge density(Q_f), equivalent oxide thickness(EOT), and gate work function. At matched gate overdrive, the dipole reduces I_{on} by less than 1 %, while obtaining the same shifts by uniformly reducing the 2DHG density would reduce it by 15 % and 31 %. Finally, we present a V_t design window which is expressed as a single boundary condition of the product of Q_f and EOT.

Keywords: Aluminum oxide, Diamond, Hafnium oxide, High-k dielectric materials, Lanthanum oxide

1 Introduction

DIAMOND FETs are promising candidates for switches for the next generation electronics due to the remarkable intrinsic properties of diamond including a critical electric field of 10–20 MV/cm, high bulk carrier mobility (2800 $cm^2/V{\cdot}s$ for electrons and 2100 $cm^2/V{\cdot}s$ for holes) and the best thermal conductivity for a bulk material (22 $W/cm{\cdot}K$[1]). It has an almost negligible intrinsic carrier concentration owing to ultra-wide bandgap. When the diamond surface is H-terminated, it forms a 2DHG through surface transfer doping[2]. The H-termination results in the top surface forming an electrical dipole, with carbon being slightly more electronegative than hydrogen (C $\approx$ 2.55, H $\approx$ 2.20) and holding the shared electrons slightly closer. This puts the carbon side slightly negative and hydrogen side slightly positive, so the dipole points outward from the surface. An electron in the valence band of the diamond is attracted toward the H^+ end of the C–H dipole. As it crosses the dipole layer the field does positive work on it, so its potential energy drops (for an electron $U = -eV$). Now the vacuum level is the energy of an electron sitting just outside the surface of the diamond, which is the energy required to take an electron from inside the crystal to the outside and park it there. Since an electron crossing the C–H dipole loses energy on the way out, the vacuum level is lowered as shown in Fig. 1a. This drops it below the conduction band minimum, which is referred to as negative electron affinity(NEA)[3]. The magnitude of the drop Δ is set by the dipole strength, $\Delta = qdN_s/(\varepsilon_0\varepsilon_r)$, where q is the bond charge, d is the C–H spacing, and N_s is the number of bonds per unit area. Thus, H-termination reduces the ionization energy of diamond ($E_{\text{vac}} - E_v$) and so the valence band maximum is pushed up toward the vacuum level. A surface acceptor state (E_a), provided by an adsorbed molecule, is pinned to the vacuum level at an offset fixed by its own electron affinity. Because the vacuum level is lower relative to the diamond bands, this acceptor level also sits lower relative to the bands, until it ends up below the valence band maximum (E_v) of diamond. Now this acceptor state, sitting lower in energy than the top of the valence band, acts as a sink where electrons from the valence band fall in. This leaves behind holes which form a two-dimensional hole gas. The electrons that move out into the surface acceptors form a negative sheet just outside the diamond (density denoted by Q_f in simulations), while the holes they leave behind form the positive 2DHG just inside it. So an electron near that external negative sheet has to sit at higher energy than one in the bulk, and the bands that represent its energy are higher close to the surface, i.e. they bend upwards. Farther away from the surface the effect gets weaker, and hence the bands remain flat in the bulk. The band bending is thus caused by the transfer-doping charge separation, while the C–H bond dipole sets only the vacuum-level step (the NEA). The band diagram for the steps leading to formation of 2DHG is shown in Fig. 1b.

Using the 2DHG formed by H-terminating diamond and exposing it to air, lateral and vertical diamond FETs can be fabricated in which drain currents above 1 A/mm[4] have been realized. These devices conduct at zero gate bias and a positive gate voltage is needed to switch these devices off. However, for fail safe operation at the converter level a normally-off switch is desired. This is to prevent the device from being in on-state even before the gate-driver has control. In most prior work this has been achieved by modifying the channel properties through partial oxygen termination under the

gate[5] or nitrogen implantation below the channel[6]. However, these approaches reduce the 2DHG density and thereby reduce the on-current[7]. Liu et al. demonstrated that sputtered $LaAlO_3$ on ALD Al_2O_3 shows normally-off characteristics after annealing[10] at 150–350 °C, while a single Al_2O_3 layer stays normally-on under the same anneal[11], and used this to place depletion-mode and enhancement-mode devices on the same substrate[11]. The authors attributed the shift to loss of adsorbed acceptors or compensating positive charge at the oxide/oxide interface, and noted that the origin remained unclear[10]. V_t control through a fixed positive surface charge has also been studied using TCAD[8] and affects the channel similarly. Another alternative is to cascode it with a Si FET as done in GaN high electron mobility transistors (HEMTs)[9], which defeats the purpose of an all-diamond configuration.

In the current work we propose employing a dipole formed at the interface of two dielectrics to shift V_t bidirectionally. The interfacial dipole is formed due to the difference in oxygen areal density as predicted by the Kita–Toriumi model[12]. It shifts V_t without reducing the surface acceptor density that helps form the channel, and its sign reverses when the deposition order is reversed, so a single material pair can move V_t in either direction. We study the use of the interfacial dipole in Al_2O_3/HfO_2 and Al_2O_3/La_2O_3 for precise V_t targeting and normally-off operation in diamond 2DHG FETs. The work provides a mechanism that predicts the direction of the V_t shift for a given bilayer, with the magnitude set by the measured flat-band shift of the pair. Engineering V_t using dielectric dipoles has been successfully implemented in silicon logic technology[13] but has not been studied in diamond. To the best of our knowledge this is the first identification and systematic study of the dielectric dipole as a V_t control method in diamond 2DHG FETs. It enables normally-off operation without modifying the channel charge, and offers a candidate mechanism for the bilayer results of Liu et al.[10,11].

The TCAD study was performed in Silvaco Victory Device (version 2.0.1.R) and calibrated against the H-terminated diamond MISFET of Hirama et al.[4] using certain material and parameters from Wong et al.[14]. We quantify the V_t shift as a function of deposition order, gate work function, EOT, and Q_f. We show that R_{on}, g_m, and channel current remain almost invariant at matched gate overdrive with the dipole being present. Finally we provide a V_t design curve for each pair of the two bilayer dielectrics.

2 Methods

When two dielectrics with different oxygen areal densities are stacked there is a migration of oxygen ions from the region of high density to lower density within a small region at the interface only[12]. As the oxygen ions leave the dielectric with higher oxygen concentration, they leave a net positive charge on that side of the interface and the region where they move into has a net negative charge – thus forming an interface dipole. This interface dipole forms a potential step at the interface. Since the two sheets are equal and opposite, the resulting field is confined between them and neither dielectric bulk carries any additional field. The dipole therefore produces a fixed potential step V_{dip} localized at the interface, irrespective of the thickness of either

layer. When this bilayer is used as a gate dielectric, it shifts the threshold voltage without reducing the surface acceptor density that supplies the channel. The sign of the potential step reverses when deposition order is switched (Fig. 2).

Figure 3a shows a schematic of a lateral 2DHG diamond FET consisting of source and drain which form the ohmic contacts and inject/collect holes. The gate sits on top of a dielectric like Al_2O_3. It behaves as a capacitor which controls the channel current through the field its charge creates. Figure 3a is also the schematic of the device used to calibrate our simulation model and derived from Hirama et al.[4].

The device structure represents the structure fabricated by Hirama et al.[4] with certain material and transport parameters being incorporated from a previous work of Wong et al.[14] including $\varepsilon_{Al_2O_3} = 6.17$, $\mu_p = 110$ cm^2/V·s, $v_{sat_p} = 1.265 \times 10^7$ cm/s, and $\beta = 0.84$. Since Victory does not accept a negative electron affinity, the band diagram is displaced uniformly by 1.30 eV which leaves all band offsets and work-function differences, and therefore all threshold voltages, unchanged. The 2DHG is induced by a fixed negative charge sheet at the diamond surface, which represents the ionized surface acceptors of the transfer-doping mechanism. NEA is assumed to be -1.3 eV. The access regions have $Q_1 = -(4 \times 10^{13})$ /cm^2, chosen to match the Hall sheet density reported by Hirama et al.[4], while the gate region has a net interface charge of $-(1.85 \times 10^{13})$ /cm^2, obtained by adding $Q_2 = (2.15 \times 10^{13})$ /cm^2 which Wong et al.[14] attributed to modification of the Al_2O_3 during Al gate deposition.

Simulations were run without self heating (isothermally) at 300 K. Repeating the calibration with lattice self-heating enabled changes the rms agreement by less than 2 % of its value, so the two are not distinguishable at the level of this fit. Thus the isothermal solution was retained for simplicity. This is consistent with the small temperature rise as observed by Wong et al.[14] with a peak lattice temperature near 320 K at $V_D = -12$ V, due to the high thermal conductivity of diamond.

Figure 3b shows the I_d–V_{ds} plots for the experimental data from Hirama et al. and the overlay of the calibration model developed for this work which shows a close fit. In the calibration model, the charge under the gate differs from that in the access regions by Q_2. Wong et al. attributed this to the modification of the Al_2O_3 during Al gate deposition[14]. Q_2 is therefore specific to that gate metal and to a single Al_2O_3 layer, and no measured value is available for the other gate metals and the bilayer stacks studied here. Carrying it into the design structures would add an assumption that cannot be supported. For the design study we therefore use a single uniform Q_f and treat it as a design variable, varied from 2.5×10^{12} to 1.25×10^{13} cm^{-2}. The acceptor sheet is negative. But the values quoted below are its magnitude. The design structures share the geometry and transport parameters of the calibrated device and are not intended to reproduce its threshold voltage. The interface dipole in this work is represented by two sheets of opposite charges. As there is no net charge, the only electrostatic effect the sheets have on the device is a step in the electrostatic potential across the plane between the charge sheets. Everywhere else the potential remains as it would be in the absence of the dipole. According to Gauss's law, these two sheets of areal charge density, σ separated by a distance of d in a medium of permittivity, ε produce an electric field $E = \sigma/\varepsilon$. The potential step can be calculated directly by integrating the field across the distance $\Delta V = \sigma \cdot d/\varepsilon$. The dipole was defined from the 0.8 V

flat-band voltage shift reported by Son et al.[15] for Al_2O_3/HfO_2 bilayer dielectrics on GaN metal oxide semiconductor capacitor (MOSCAP) structures. Taking the distance between the sheets as 1 nm, $\sigma = 4.37 \times 10^{-6}$ C/cm^2. This dipole is formed at the interface between the two dielectrics. Assuming each sheet is distributed uniformly over a slab of 0.25 nm thickness (t), the volume charge density of this charge slab given $\rho = \frac{\sigma}{q \cdot t}$ is found to be 1.09×10^{21} cm^{-3}. Similarly, for the Al_2O_3/La_2O_3 bilayer the dipole was defined from the 1.7 V flat-band voltage shift reported by Chen et al.[16] for layers deposited on AlGaN/GaN MOSCAP structures. The σ value was found to be 9.29×10^{-6} C/cm^2 and $\rho = 2.32 \times 10^{21}$ cm^{-3}. These values were used in the simulation to simulate the effect of the interface dipole in the 2DHG FET. This volumetric representation of the charge sheets holds true because as per Gauss's law, the field outside the pair of charge sheets will only depend on the total charge enclosed by them. Because the net charge of the dipole is zero, representing it as two charge sheets or as two volumetric slabs is equivalent. Since an interfacial dipole layer introduces an abrupt, localized potential step across a dielectric interface, the resulting flat band voltage shift is directly correlated to this potential step.

To verify the effect of the dipole on the device stack the potential step created by the dipole can be compared to the flat band voltage shift used to calculate the charge density of the dipole. It is essential to isolate the contribution of the dipole. Otherwise, the potential profile exhibits ramps on both sides of the dipole sheets, making the true step difficult to extract. To overcome this, two devices with identical dielectric stacks, Al_2O_3 on bottom (10 nm thickness) and HfO_2 on top (10 nm thickness), one containing the interfacial charge (termed as Dipole ON) and one without charge (Dipole OFF) were simulated. The Dipole OFF device had a $V_t = 1.32$ V and the Dipole ON device had a $V_t = 0.48$ V. The devices were biased at $V_G = V_t - \Delta V$ to have identical electrostatic conditions. Vertical cutlines beneath the gate provided potential profiles, and subtracting the Dipole OFF potential from the Dipole ON potential at identical depths shows a clean interfacial step. The extracted potential step of $\sim$0.85 V agrees with the 0.8 V flat-band shift used to define the dipole. Similarly for the La_2O_3/Al_2O_3 device, the Dipole OFF device had a $V_t = 1.28$ V and for Dipole ON it was $V_t = -0.51$ V. In this case the extracted potential step was $\sim$1.79 V which is close to the value of the flat band shift of 1.7 V. With the reverse Dipole ON stack in La_2O_3/Al_2O_3 (Al_2O_3 on top) the V_t was 3.09 V. The extracted potential steps are shown in Fig. 4.

The threshold voltage was extracted using the constant current method. Constant current method is one of the widely used methods to extract V_t[17]. V_{DS} is usually kept below 100 mV, while grounding the source and body terminals. Threshold voltage is extracted to be the gate bias at which current reaches a particular current value (I_{const}). Here we consider a commonly used value for $I_{const} = 100$ nA. Plugging it into the equation below we get $I_D = 4.54 \times 10^{-8}$ A.

$$I_D = \frac{W}{L} I_{\text{const}} \tag{1}$$

Where $W = 1$ μm (channel width) and $L = 2.2$ μm (channel length).

3 Results

Three distinct dipoles appear in this device and should be clearly distinguished – 1) The C–H bond dipole at the diamond surface : This sets the vacuum-level step and hence is responsible for the negative electron affinity at the diamond surface. It sets the energetic condition for transfer doping without transferring charge. 2) The charge separation produced by transfer doping: This is created by the electrons in the surface adsorbate layer and holes in the diamond and creates the 2DHG and the upward band bending. It fixes the channel sheet density. 3) The interface dipole at the boundary of the bilayer dielectrics: It forms at the internal boundary between the two oxides of the gate stack, arises from the difference in oxygen areal density across that boundary, and produces a potential step within the dielectric. For the subsequent analysis eleven different gate dielectric stacks were used consisting of Al_2O_3 only, HfO_2 only, La_2O_3 only, bilayer stacks of Al_2O_3/HfO_2 and Al_2O_3/La_2O_3 with deposition order reversed with both Dipole ON and Dipole OFF configurations. Q_f was taken as 2.5×10^{12} /cm^2 for all subsequent simulations apart from the Q_f skew study. For all of the plots magnitude of the Q_f was used.

Figure 4b shows the I_d–V_{gs} plot for the diamond 2DHG FET with Al_2O_3 dielectric, and Dipole ON condition for the Al_2O_3/HfO_2 and Al_2O_3/La_2O_3 bilayer structures. It shows a clear shift in the transfer characteristics along with shift in threshold voltage. The metal-semiconductor work function difference is given by[18] :

$$\begin{aligned} \phi_{ms} &= \phi_m - \left(\chi + \frac{E_g}{2q} + \psi_{Bp}\right) \\ &= \phi_m - \left(\chi + \frac{E_g}{q} - \phi_p\right) \end{aligned} \tag{2}$$

ϕ_m is the gate metal work function, χ is electron affinity, ψ_{Bp} is the bulk Fermi potential measured from mid-gap, and ϕ_p is the Fermi potential measured from valence band edge or $\psi_{Bp} = \frac{E_g}{2q} - \phi_p$. The flat band voltage is given by the equation :

$$V_{FB} = \phi_{ms} - \frac{Q_f + Q_m + Q_{ot}}{C_{ox}} \tag{3}$$

Where C_{ox} is the capacitance per unit area of the dielectric, Q_f is the fixed oxide charge, Q_m is the mobile ionic charge, and Q_{ot} is the oxide trapped charge. For the scope of the present study we do not consider any mobile ionic charge or trapped charges and therefore,

$$V_{FB} = \phi_{ms} - \frac{Q_f}{C_{ox}} \tag{4}$$

In the present study instead of SiO_2, we have two dielectric pairs, Al_2O_3/HfO_2 and Al_2O_3/La_2O_3. These dielectrics would have capacitances in series and for expressing the effective thickness in terms of the equivalent thickness of the SiO_2 we use the EOT

by dividing by the ratio of dielectric constant and multiplying by the thickness

$$\mathrm{EOT} = \frac{\kappa_{\mathrm{SiO_2}}}{\kappa_{\mathrm{Al_2O_3}}} t_{\mathrm{Al_2O_3}} + \frac{\kappa_{\mathrm{SiO_2}}}{\kappa_{\mathrm{HfO_2}}} t_{\mathrm{HfO_2}} \tag{5}$$

$$\mathrm{EOT} = \frac{\kappa_{\mathrm{SiO_2}}}{\kappa_{\mathrm{Al_2O_3}}} t_{\mathrm{Al_2O_3}} + \frac{\kappa_{\mathrm{SiO_2}}}{\kappa_{\mathrm{La_2O_3}}} t_{\mathrm{La_2O_3}} \tag{6}$$

For a normal inversion channel MOSFET[18],

$$\begin{aligned} V_t &= V_{FB} + 2\psi_B + \frac{\sqrt{2\varepsilon_s q N_A (2\psi_B)}}{C_{ox}} \\ &= \left(\phi_{ms} - \frac{Q_f}{C_{ox}}\right) + 2\psi_B + \frac{\sqrt{4\varepsilon_s q N_A \psi_B}}{C_{ox}} \end{aligned} \tag{7}$$

The second term corresponds to the surface potential required to reach strong inversion, and the third to the depletion charge uncovered in reaching it. Neither has a counterpart in the present device since the body is p-type from unintentional boron incorporation and the channel is a hole gas, so channel and body carriers are of the same type and the device operates in accumulation rather than inversion. The flat-band term is independent of the inversion condition and thus present. Threshold is defined by the Fermi level at the channel interface reaching the band edge, rather than by inversion criterion. Hence for the particular device,

$$V_t \approx \phi_{ms} + \frac{qQ_f}{C_{ox}} \tag{8}$$

Where Q_f is the magnitude of the equilibrium 2DHG sheet density at zero gate bias, and the ionized adsorbate acceptors that induce the channel are equal in areal density to the transferred holes, so they are accounted for through Q_f and do not appear as a separate fixed-charge term. The change in $\mathrm{V_t}$ using a dipole was studied as a function of three known control knobs (ϕ_{ms}, EOT, and $\mathrm{Q_f}$) which can modify the threshold voltage and the potential step introduced by the dipole.

$$\frac{\partial V_t}{\partial \phi_{ms}} = 1 \tag{9}$$

$$\frac{\partial V_t}{\partial V_{dip}} = 1 \tag{10}$$

$$\frac{\partial V_t}{\partial \mathrm{EOT}} = \frac{qQ_f}{\varepsilon_0 \kappa_{\mathrm{SiO_2}}} \tag{11}$$

$$\frac{\partial V_t}{\partial Q_f} = \frac{q}{C_{ox}} = \frac{q \cdot \mathrm{EOT}}{\varepsilon_0 \kappa_{\mathrm{SiO_2}}} \tag{12}$$

Figures 5a, 5b show the effect of modifying the work function on the $\mathrm{V_t}$. As expected with increase in metal work function, $\mathrm{V_t}$ increases due to the change in $\mathrm{V_{FB}}$ (equation (9)).

We chose four metals for this study : $\Phi_{Al} = 4.28$ eV, $\Phi_{TiN} = 4.6$ eV, $\Phi_{Ni} = 5.15$ eV, and $\Phi_{Pt} = 5.65$ eV. For a given metal work function, it was found that adding the interface dipole changed the V_t depending on the deposition order. For example, with an Al gate on Al_2O_3 alone, $V_t = 1.1$ V. If an interface dipole charge is added i.e. Al_2O_3 (bottom) + HfO_2 (top) [Dipole ON], the V_t is 0.48 V. The Dipole OFF condition represents the case as mentioned earlier when the interface charge is not taken into the model and thus the change in threshold voltage is due to change in EOT. Hence the two curves overlap in Fig. 5a and 5b for both the Dipole OFF pairs. Similar trends were observed across all metals and all dielectric stacks. With the Dipole OFF condition the $V_t = 1.32$ V hence $\Delta V_t = 0.84$ V is observed between Dipole OFF and ON. If the deposition order is reversed i.e. Al_2O_3 (top) + HfO_2 (bottom) [Dipole ON] the V_t is 2.18 V, whereas the Dipole OFF condition V_t is 1.33 V Hence, the difference between Dipole ON and OFF $\Delta V_t = -0.84$ V. Similarly the difference between Dipole OFF and ON in the Al_2O_3/La_2O_3 stack is ± 1.79 V (Fig. 5c).

Following this, the EOT was varied by modifying the thickness of the two dielectrics. The thickness of the two dielectrics for a particular dipole pair was kept equal. The thickness of each layer was varied from 2.5 nm to 12.5 nm in steps of 2.5 nm. Figures 6a and 6b show the effect of change of EOT on V_t. Equal thicknesses of Al_2O_3 and HfO_2/La_2O_3 were taken from 2.5 nm to 12.5 nm each in step of 2.5 nm. The corresponding combined EOT thickness was calculated using equations (5) and (6). Thus, the combined thicknesses corresponded to EOT thickness of 2.02 nm, 4.05 nm, 6.07 nm, 8.09 nm, and 10.12 nm respectively using equations (5) and (6). The dielectric constants used were: $\kappa_{Al_2O_3} = 6.17$ ref. 14, $\kappa_{HfO_2} = 22$ (same as calibration model) and $\kappa_{La_2O_3} = 27$. As EOT increases threshold voltage increases. For a given EOT, depending on the dipole order the threshold voltage moves by ∼0.84 V between the Dipole ON and OFF conditions. Finally, increasing the acceptor density Q_f that induces the 2DHG raises V_t (Fig. 6c), as predicted by equation (12).

4 Discussion

When modulating the threshold voltage, if the method used reduces the 2DHG, it results in degradation in R_{on} since the ungated access regions between the contacts and the gate are not modulated by the gate and have the sheet resistance provided by the surface charge.

$$R_{on}W = 2R_cW + R_gW + \frac{L_{GS} + L_{GD}}{q\mu_p Q_f} \tag{13}$$

where the first term is the contact resistance, second is the gated channel resistance whose charge is controlled by the gate overdrive, and the third is the access-region sheet resistance with $p_s = Q_f$. Plotted against $1/Q_f$, the access term is a straight line through the origin with slope $L_{access}/(q\mu_p)$.

Figure 7a shows the R_{on} vs $1/Q_f$ plot where R_{on} is calculated at 5 V overdrive ($V_t - 5$ V) for each Q_f in the sweep and plotted against $1/Q_f$ so that a change in Q_f moves R_{on} along the line, whereas anything that doesn't affect the access regions can only move the intercept. All four stacks, both dielectric pairs with the Dipole ON and

off, fall on lines with slopes of (0.96–1.04) $\times 10^{14}$ k$\Omega \cdot \mu$m/cm^2. The value expected from the access geometry with $L_{GS} + L_{GD} = 1.8$ μm and $\mu_p = 110$ cm^2/V·s, is 1.02×10^{14} k$\Omega \cdot \mu$m/cm^2, so the slope is the access-region sheet resistance, which the dipole does not change. The Dipole ON lines sit at most 2 % (Al_2O_3/HfO_2) and 5 % (Al_2O_3/La_2O_3) above the Dipole-OFF lines over the entire Q_f range, and this small excess arises from the gated channel operating at slightly reduced overdrive, since the channel charge is unchanged. A method that removes surface acceptors over the whole surface, including the access regions, moves the device along this line to higher $1/Q_f$ and therefore higher R_{on}, whereas the dipole leaves its position on the line unchanged. The dipole shifts V_t by 0.84 and 1.79 V and does not move the slope at all, because the potential step is confined to the gate stack and does not extend into the access regions.

While R_{on} is dominated by the access regions, transconductance (g_m) is determined by the gated channel. Here we take $V_{ds} = -0.1$ V. Thus $g_m = \frac{dI_d}{dV_{gs}}\Big|_{V_{ds}=-0.1\,\mathrm{V}}$. Gate voltage was swept from -10 V to $+4$ V in steps of 0.1 V, and g_m was computed as the difference quotient of I_d between successive bias points. Figure 7b shows g_m at a matched overdrive of $V_g - V_t = -5$ V, for different Q_f values for both dielectric pairs with the Dipole ON and off. Since the abscissa is $V_g = V_t - 5$ V, the Dipole-ON points are 0.84 V and 1.79 V from the Dipole-OFF points. At matched overdrive the dipole changes g_m by less than 5 % for $Q_f \geq 5 \times 10^{12}$ /cm^2 in both pairs (-4 % to $+0.3$ % for Al_2O_3/HfO_2 and -2 % to -5 % for Al_2O_3/La_2O_3), while the Dipole-OFF points almost coincide (differ slightly due to EOT difference). The difference grows as Q_f is reduced, reaching 10 % for Al_2O_3/La_2O_3 at (2.5×10^{12} /cm^2), where the access region resistance is the largest and takes the greatest share of applied bias. The dipole therefore acts as a fixed offset to the gate voltage. Mobility and gate capacitance are unaffected, so the device is equivalent to one with a different gate-metal work function. Previous techniques for achieving normally-off devices do not work as well as the current method. The partial C–O channel of Kitabayashi et al.[5] has a sheet resistance of (1–5) $\times 10^5$ Ω/sq, one to two orders of magnitude above that of the C–H surface, and its current is limited by the low mobility of the C–O channel. The nitrogen-implanted device implemented by Oi et al.[6] has a sheet resistance of (2–8) $\times 10^5$ Ω/sq, whereas the C–H samples without nitrogen-implantation have (4–10) $\times 10^4$ Ω/sq of sheet resistance. The current density in the nitrogen-implanted devices is one to two orders of magnitude less than that of normally-on devices. The current loss can be partly attributed to the overdrive, as the V_t shifts around 20 V[6]. Even if the whole shift is considered as lost overdrive at $V_{gs} = -30$ V, the overdrive is lowered only from 47.5 V to 27.5 V. Comparing the two at equal gate overdrive would raise the current by a factor of 1.7 if the current scales linearly with overdrive, and by a factor of 3.0 if it scales quadratically. Applying this criterion to the one to two orders of current-reduction reported by Oi et al.[6], the implanted devices carry only 2–30 % of the current of the normally-on device at matched overdrive. In contrast, the dipole changes the on-current by less than 1 % at matched overdrive. Neither methods provide an way to reproduce a device of a certain V_t. In the partial C–O channel

devices, V_t varied from -2.5 V to -4 V across three devices, whereas in the nitrogen-implanted devices, 55 %–75 % of devices were normally-off. Whereas the dipole shift does not depend on Q_f, EOT or gate metal.

The two routes to moving V_t, adding the dipole and reducing Q_f, can be compared by plotting the on-current against the V_t shift each produces. Figure 7c plots the normalized drain current at a gate overdrive of $V_g - V_t = -5$ V and the ΔV_t. Within each dielectric pair, the current is normalized with respect to the drain current of the Dipole-OFF case at $Q_f = 1.25 \times 10^{13}$ /cm^2 and ΔV_t calculated with respect to its V_t, hence the reference sits at (0,1) for $Q_f = -1.25 \times 10^{13}$ /cm^2. Each curve is a sweep of Q_f from (2.5×10^{12} /cm^2) to (1.25×10^{13} /cm^2). Moving along a curve corresponds to reducing Q_f, and moving between curves at the same height corresponds to adding the dipole. Vertical axis therefore shows the current lost and the horizontal axis the V_t shift gained.

Moving along a curve is costly – reducing Q_f by a factor of five shifts Vt by 3.77 V (Al_2O_3/HfO_2) and 3.61 V (Al_2O_3/La_2O_3) but retains only 28 % of the original current, because the ungated access regions lose sheet charge in proportion. The dipole instead displaces the whole curve horizontally: at matched current the Al_2O_3/HfO_2 dipole shifts V_t by 0.84 ± 0.01 V and the Al_2O_3/La_2O_3 dipole by 1.79 V, and in both cases the shift is the same at every Qf, confirming that it is independent of the channel charge. Obtaining those shifts by reducing Q_f alone would cost about 15 % and 31 % of the on-current respectively. With the dipole, the on-current at the highest Q_f is within 0.1 % (Al_2O_3/HfO_2) and 0.9 % (Al_2O_3/La_2O_3) of the dipole-off value. Figure 7c therefore serves as a design curve – for a target V_t, it identifies the Q_f and stack combination that reaches it at the highest current. The V_t for the 2DHG diamond FET from Equation (8) can be written as:

$$V_t = \phi_{ms} + \frac{qQ_f}{C_{ox}} \tag{14}$$

Where Q_f is the magnitude of the interface charge density. Expressing the gate capacitance through the equivalent oxide thickness $C_{ox} = \varepsilon_0 \kappa_{SiO_2}/\mathrm{EOT}$.

Thereby we can write :

$$V_t = \phi_{ms} + \frac{q \cdot Q_f\,\mathrm{EOT}}{\varepsilon_0 \kappa_{SiO_2}} \tag{15}$$

The dipole adds a fixed potential step, which is independent of both EOT and Q_f. Thus we can write :

$$V_t = \phi_{ms} + \frac{qQ_f \cdot \mathrm{EOT}}{\varepsilon_0 \kappa_{SiO_2}} + sV_{dip} \tag{16}$$

With $s = 0$ without a dipole $s = -1$ when Al_2O_3 is the bottom layer and $s = +1$ when Al_2O_3 is on top. Equation (16) shows that EOT and Q_f enter the V_t expression as a product, and hence the two dimensional design space reduces to a single variable which is the product $Q_f \times \mathrm{EOT}$. Fitting the extracted threshold voltages for the Al_2O_3/HfO_2

pair against this product for a range of Q_f and EOT we get :

$$V_{t\text{-Dipole OFF}} = 0.0466\,(\text{EOT} \times Q_f) + 0.372 \tag{17}$$
$$V_{t\text{-Dipole ON}} = 0.0466\,(\text{EOT} \times Q_f) - 0.47 \tag{18}$$

Similarly, for Al_2O_3/La_2O_3

$$V_{t\text{-Dipole OFF}} = 0.0466\,(\text{EOT} \times Q_f) + 0.381 \tag{19}$$
$$V_{t\text{-Dipole ON}} = 0.0466\,(\text{EOT} \times Q_f) - 1.41 \tag{20}$$

Where Q_f is in units of 10^{12} /cm^2. The common slope agrees with the analytic coefficient $q/(\varepsilon_0\kappa_{SiO_2}) = 0.0464$ V/(nm·10^{12} /cm^2) to within 0.4 %, confirming that the simulated threshold follows (15). Since both cases share the same slope, it confirms that the dipole is independent of EOT and Q_f, and the intercepts differ by 0.84 V and 1.79 V, equal to the extracted dipole shift. Now to compute a design space for V_t, the Q_f was varied from 1×10^{12} to 1.3×10^{13} /cm^2 and EOT was varied from 1 to 10 nm. Using the product we are able to predict the V_t using equations (17)–(20) and able to generate contour plots for Dipole ON and Dipole OFF conditions for both Al_2O_3/HfO_2 and Al_2O_3/La_2O_3 structures as shown in Fig. 8.

The Dipole-OFF maps contain no normally-off region, as equations (17) and (19) predict. Normally-off operation in this device requires $V_t < 0$. Without the dipole the intercept is positive, so $V_t \geq 0.372$ V and $V_t \geq 0.381$ V for every combination of EOT and Q_f, for Al_2O_3/HfO_2 and Al_2O_3/La_2O_3 structures respectively. No point in the design space gives a normally-off device with Dipole-OFF. With the Dipole ON the intercept becomes negative and the condition which defines the boundary $V_t < 0$ is:

$$\text{EOT} \cdot Q_f < \frac{V_{dip} - \phi_{ms}}{q/\varepsilon_0\kappa_{SiO_2}} \tag{21}$$

which is a hyperbola in the EOT–Q_f plane. For Al_2O_3/HfO_2 this gives EOT $\cdot\, Q_f <$ 10 nm·10^{12} /cm^2, and for Al_2O_3/La_2O_3, EOT $\cdot\, Q_f < 30.26$ nm·10^{12} /cm^2 which is shown in the contour plot bounded by the dashed contour, and the window grows with the dipole strength. At $Q_f = 2.5 \times 10^{12}$ /cm^2 Al_2O_3/HfO_2 permits EOT up to 4.0 nm, while Al_2O_3/La_2O_3 permits the full 10 nm range simulated. At $Q_f = 1.3 \times 10^{13}$ /cm^2, Al_2O_3/HfO_2 requires EOT below 0.8 nm, which is not practical, whereas Al_2O_3/La_2O_3 allows up to 2.3 nm.

5 Conclusion

Thus in this study, we have proposed and quantified the dielectric interface dipole as a threshold voltage control for hydrogen-terminated diamond 2DHG FETs. Because the dipole is charge-neutral, it contributes a fixed potential step that adds directly to the threshold voltage in the same way as the gate work function, and is therefore independent of equivalent oxide thickness, interface charge, and gate metal. We find shifts of 0.84 V for Al_2O_3/HfO_2 and 1.79 V for Al_2O_3/La_2O_3, reversing in sign with

deposition order. At matched overdrive the dipole costs less than 1 % of the on-current, whereas achieving the same shifts by uniformly lowering Q_f costs 15–31 %, and nitrogen implantation costs 70–98 %. Normally-off operation becomes a condition of the product $Q_f \times EOT$ which is unattainable without a dipole. These results also offer a candidate mechanism for the annealed bilayer stacks of Liu et al.[10], for which the origin of the shift was not identified.

Supplementary information. Not applicable.

Acknowledgements. The authors would like to thank Prof. Marc M. Cahay for his valuable inputs for improving the manuscript.

Declarations

Funding. This work was supported by the startup funding of M.D. from The University of Texas at San Antonio.

Competing interests. The authors declare no competing interests.

Ethics approval and consent to participate. Not applicable.

Consent for publication. Not applicable.

Data availability. Data generated during the current study are available from the corresponding author on reasonable request.

Materials availability. Not applicable.

Code availability. The Silvaco Victory Device input decks used in this study are available from the corresponding author on reasonable request.

Author contributions. A.D.U. performed the TCAD simulations. M.D. conceived the study and helped prepare the figures. Both authors analyzed the results and contributed to writing the manuscript.

References

1. Wort, C. J. H. & Balmer, R. S. Diamond as an electronic material. *Mater. Today* **11**(1–2), 22–28. https://doi.org/10.1016/S1369-7021(07)70349-8 (2008).

2. Maier, F., Riedel, M., Mantel, B., Ristein, J. & Ley, L. Origin of surface conductivity in diamond. *Phys. Rev. Lett.* **85**(16), 3472–3475. https://doi.org/10.1103/PhysRevLett.85.3472 (2000).

3. Cui, J. B., Ristein, J. & Ley, L. Electron affinity of the bare and hydrogen covered single crystal diamond (111) surface. *Phys. Rev. Lett.* **81**(2), 429–432. https://doi.org/10.1103/PhysRevLett.81.429 (1998).

4. Hirama, K., Sato, H., Harada, Y., Yamamoto, H. & Kasu, M. Diamond field-effect transistors with 1.3 A/mm drain current density by Al_2O_3 passivation layer. *Jpn. J. Appl. Phys.* **51**(9R), 090112. https://doi.org/10.1143/JJAP.51.090112 (2012).

5. Kitabayashi, Y. et al. Normally-off C–H diamond MOSFETs with partial C–O channel achieving 2-kV breakdown voltage. *IEEE Electron Device Lett.* **38**(3), 363–366. https://doi.org/10.1109/LED.2017.2661340 (2017).

6. Oi, N. et al. Normally-off two-dimensional hole gas diamond MOSFETs through nitrogen-ion implantation. *IEEE Electron Device Lett.* **40**(6), 933–936. https://doi.org/10.1109/LED.2019.2912211 (2019).

7. Li, M. et al. Recent advances in diamond MOSFETs with normally off characteristics. *Funct. Diamond* **4**(1), 2357654. https://doi.org/10.1080/26941112.2024.2357654 (2024).

8. Alhasani, R. et al. An enhanced two-dimensional hole gas (2DHG) C–H diamond with positive surface charge model for advanced normally-off MOSFET devices. *Sci. Rep.* **12**, 4203. https://doi.org/10.1038/s41598-022-05180-4 (2022).

9. Huang, X., Liu, Z., Li, Q. & Lee, F. C. Evaluation and application of 600 V GaN HEMT in cascode structure. *IEEE Trans. Power Electron.* **29**(5), 2453–2461. https://doi.org/10.1109/TPEL.2013.2276127 (2014).

10. Liu, J. W. et al. Control of normally on/off characteristics in hydrogenated diamond metal-insulator-semiconductor field-effect transistors. *J. Appl. Phys.* **118**(11), 115704. https://doi.org/10.1063/1.4930294 (2015).

11. Liu, J. et al. Logic circuits with hydrogenated diamond field-effect transistors. *IEEE Electron Device Lett.* **38**(7), 922–925. https://doi.org/10.1109/LED.2017.2702744 (2017).

12. Kita, K. & Toriumi, A. Origin of electric dipoles formed at high-k/SiO_2 interface. *Appl. Phys. Lett.* **94**(13), 132902. https://doi.org/10.1063/1.3110968 (2009).

13. Arimura, H. et al. Dipole-first gate stack as a scalable and thermal budget flexible multi-Vt solution for nanosheet/CFET devices. In *2021 IEEE International Electron Devices Meeting (IEDM)* 13.5.1–13.5.4. https://doi.org/10.1109/IEDM19574.2021.9720527 (IEEE, 2021).

14. Wong, H. Y., Braga, N. & Mickevicius, R. V. Prediction of highly scaled hydrogen-terminated diamond MISFET performance based on calibrated TCAD simulation. *Diam. Relat. Mater.* **80**, 14–17. https://doi.org/10.1016/j.diamond.2017.10.004 (2017).

15. Son, J., Chobpattana, V., McSkimming, B. M. & Stemmer, S. Fixed charge in high-k/GaN metal-oxide-semiconductor capacitor structures. *Appl. Phys. Lett.* **101**(10), 102905. https://doi.org/10.1063/1.4751466 (2012).

16. Chen, Y.-H. et al. Flat band voltage modulation of AlGaN/GaN MOS capacitor with stacked Al_2O_3/La_2O_3 high dielectric structures. *Mater. Sci. Semicond.*

Process. **48**, 9–13. https://doi.org/10.1016/j.mssp.2016.03.004 (2016).

17. Ortiz-Conde, A. et al. A review of recent MOSFET threshold voltage extraction methods. *Microelectron. Reliab.* **42**(4–5), 583–596. https://doi.org/10.1016/S0026-2714(02)00027-6 (2002).

18. Sze, S. M. & Ng, K. K. *Physics of Semiconductor Devices* 3rd edn (Wiley, 2007).

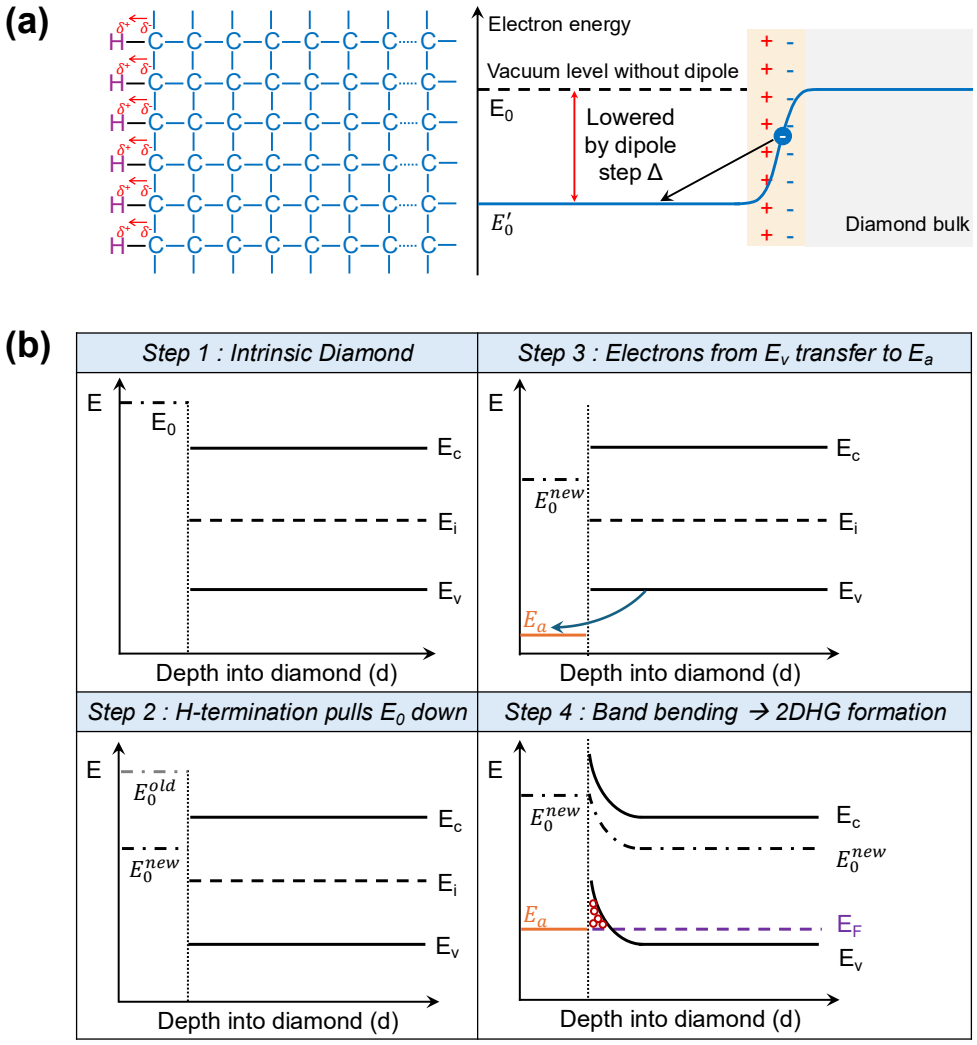


Fig. 1 **(a)** H-termination of diamond leading to negative electron affinity. **(b)** Band diagram (not to scale) showing formation of 2DHG

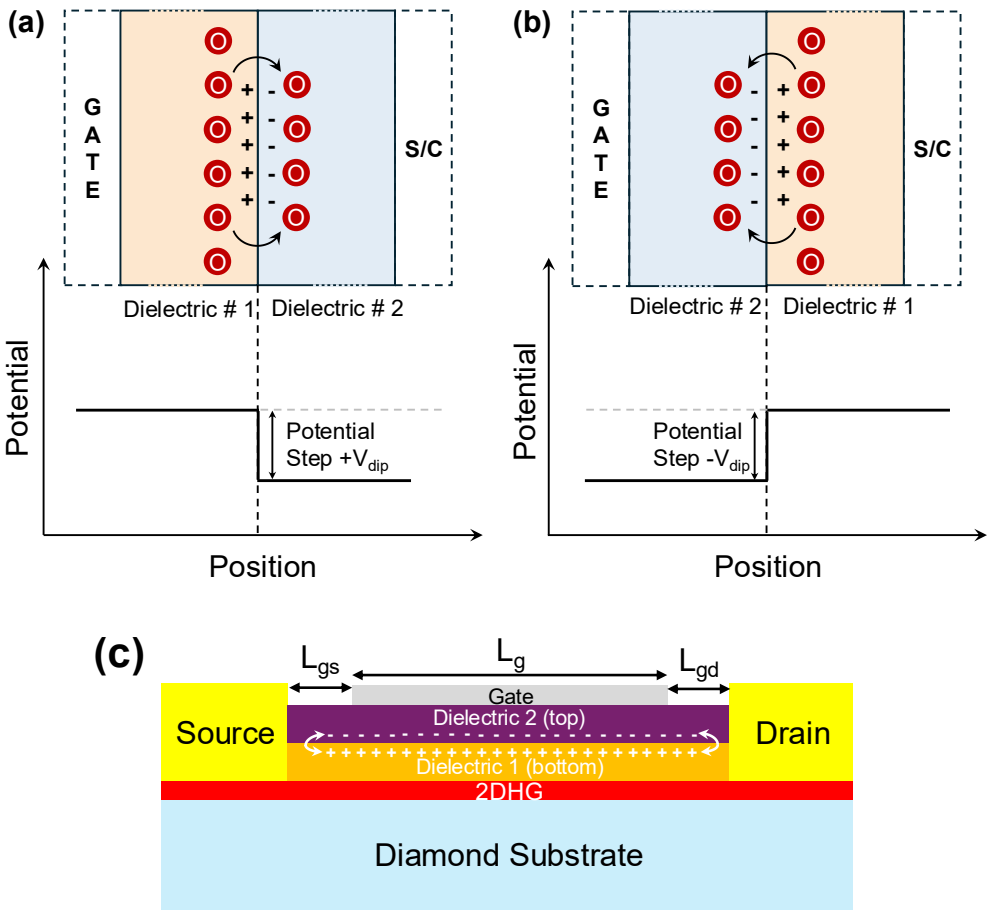


Fig. 2 Dielectric dipole formation and potential step. Dielectric # 1 has more oxygen areal density than dielectric # 2 and produces a potential step $+V_{dip}$ when dielectric # 2 makes contact to the semiconductor (S/C) **(a)** and $-V_{dip}$ when deposition order is reversed **(b)**, where V_{dip} denotes resulting potential shift, **(c)** Device schematic for diamond 2DHG FET with dielectric dipole

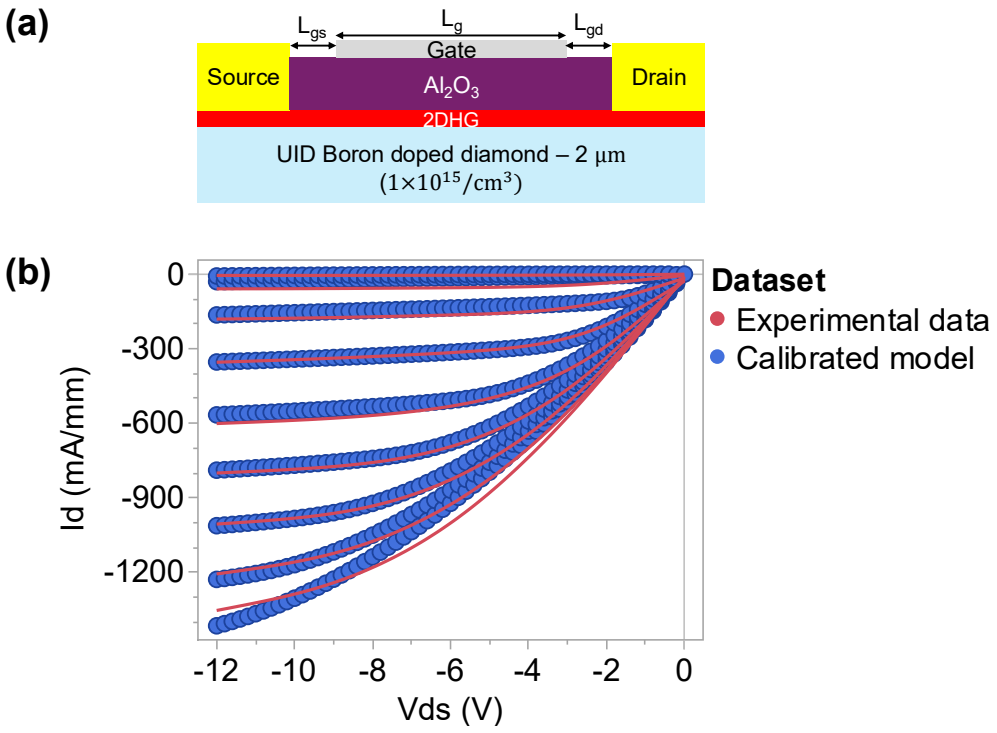


Fig. 3 **(a)** Schematic of the device used for calibration, adapted from Wong et al.[14] for the diamond 2DHG FET of Hirama et al.[4] (not to scale). **(b)** I_d–V_{ds} characteristics: experimental data of Hirama et al.[4] and the calibration model used in this study. V_{gs} varies from −5 V to 9 V in steps of −2 V.

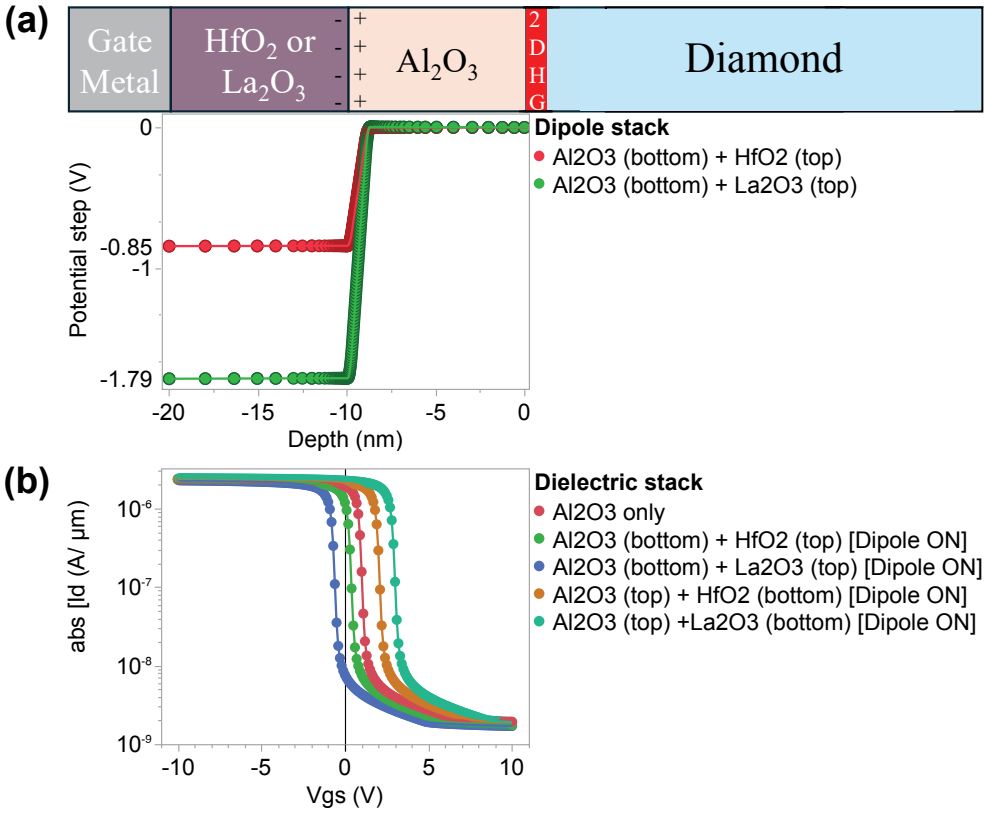


Fig. 4 **(a)** Potential step due to interface dipole **(b)** I_d–V_{gs} characteristics of device for different gate stacks

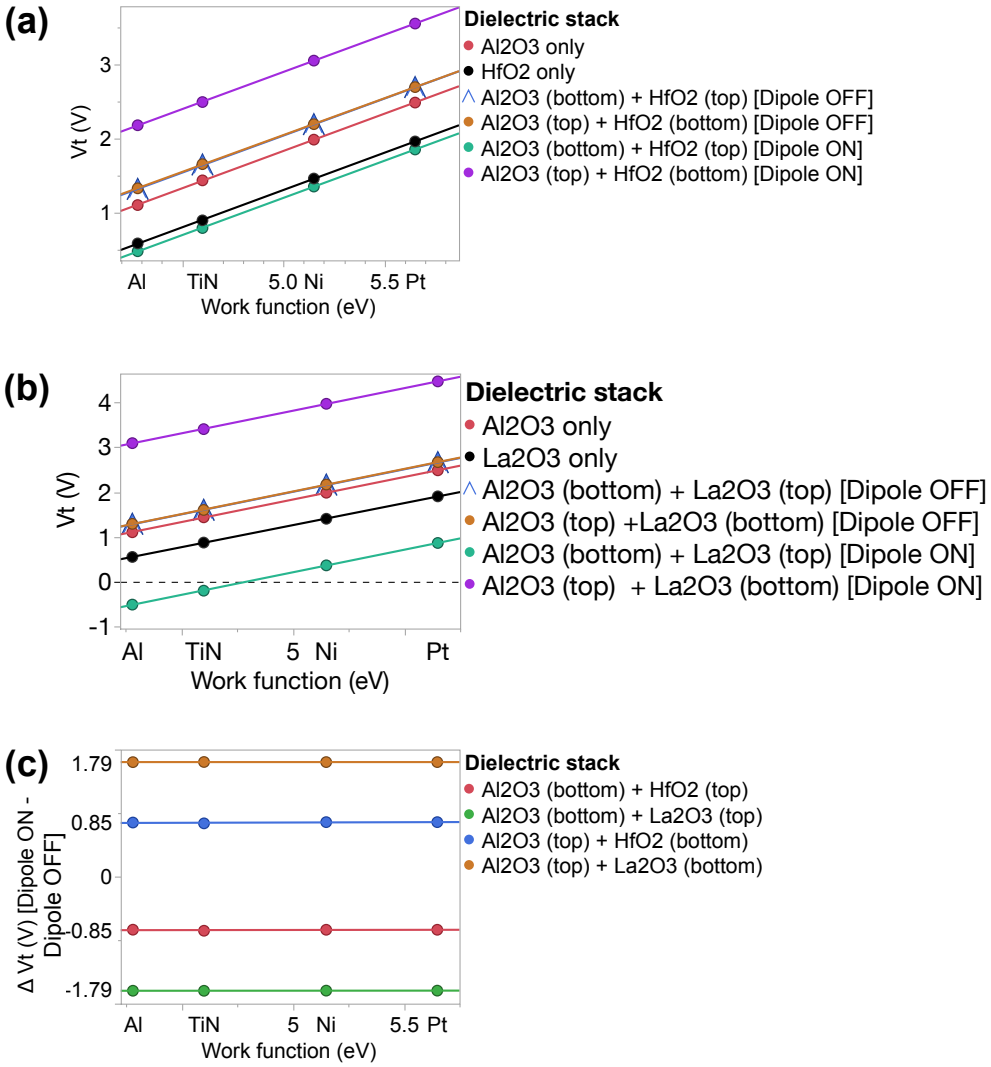


Fig. 5 **(a)** Work function vs V_t for various gate stacks of Al_2O_3/HfO_2 **(b)** Work function vs V_t for various gate stacks of Al_2O_3/La_2O_3 **(c)** ΔV_t between Dipole ON and OFF for the two dipole pairs

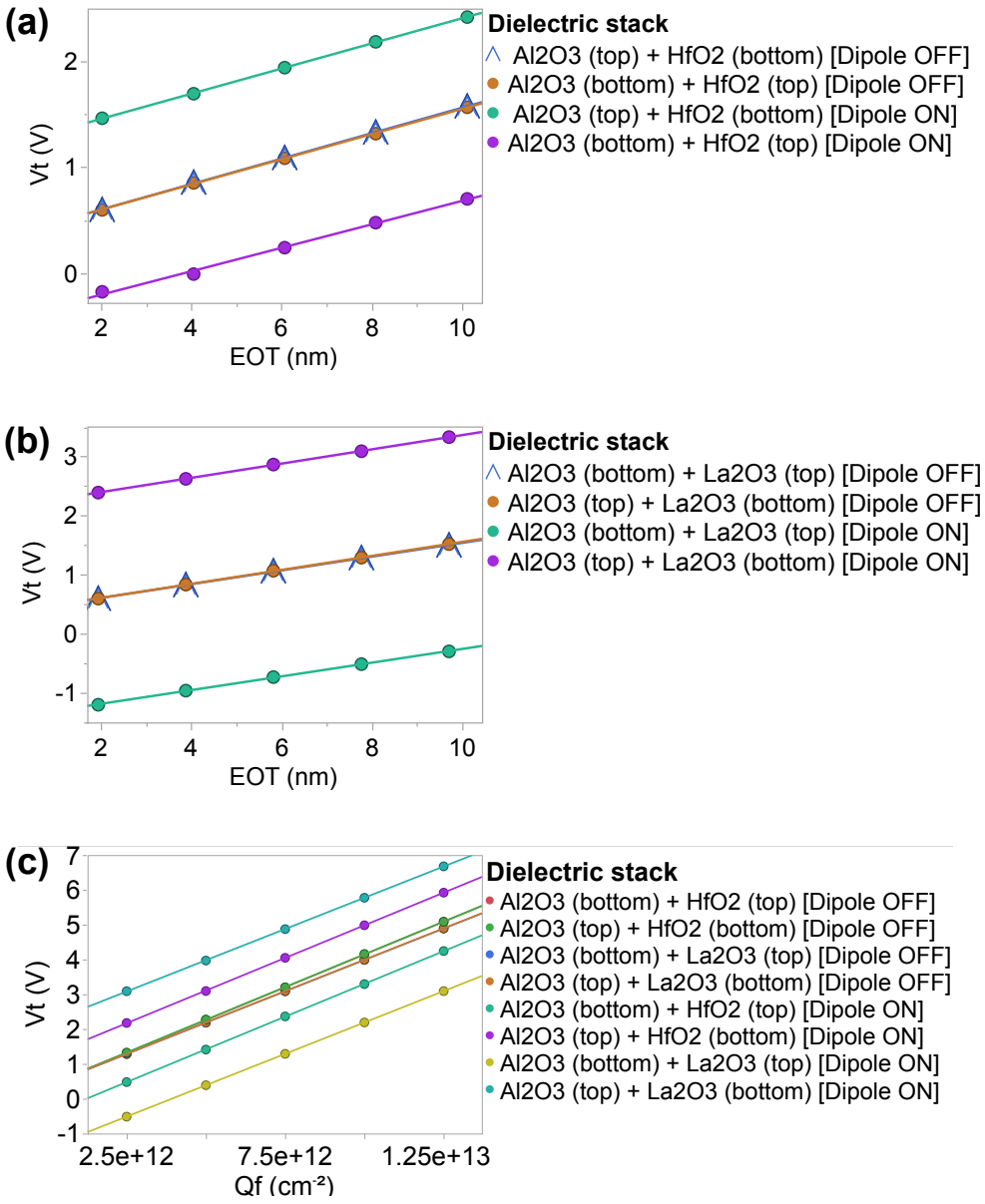


Fig. 6 **(a)** EOT vs V_t for various gate stacks of Al_2O_3/HfO_2 **(b)** EOT vs V_t for various gate stacks of Al_2O_3/La_2O_3 **(c)** Q_f vs V_t for various gate stacks

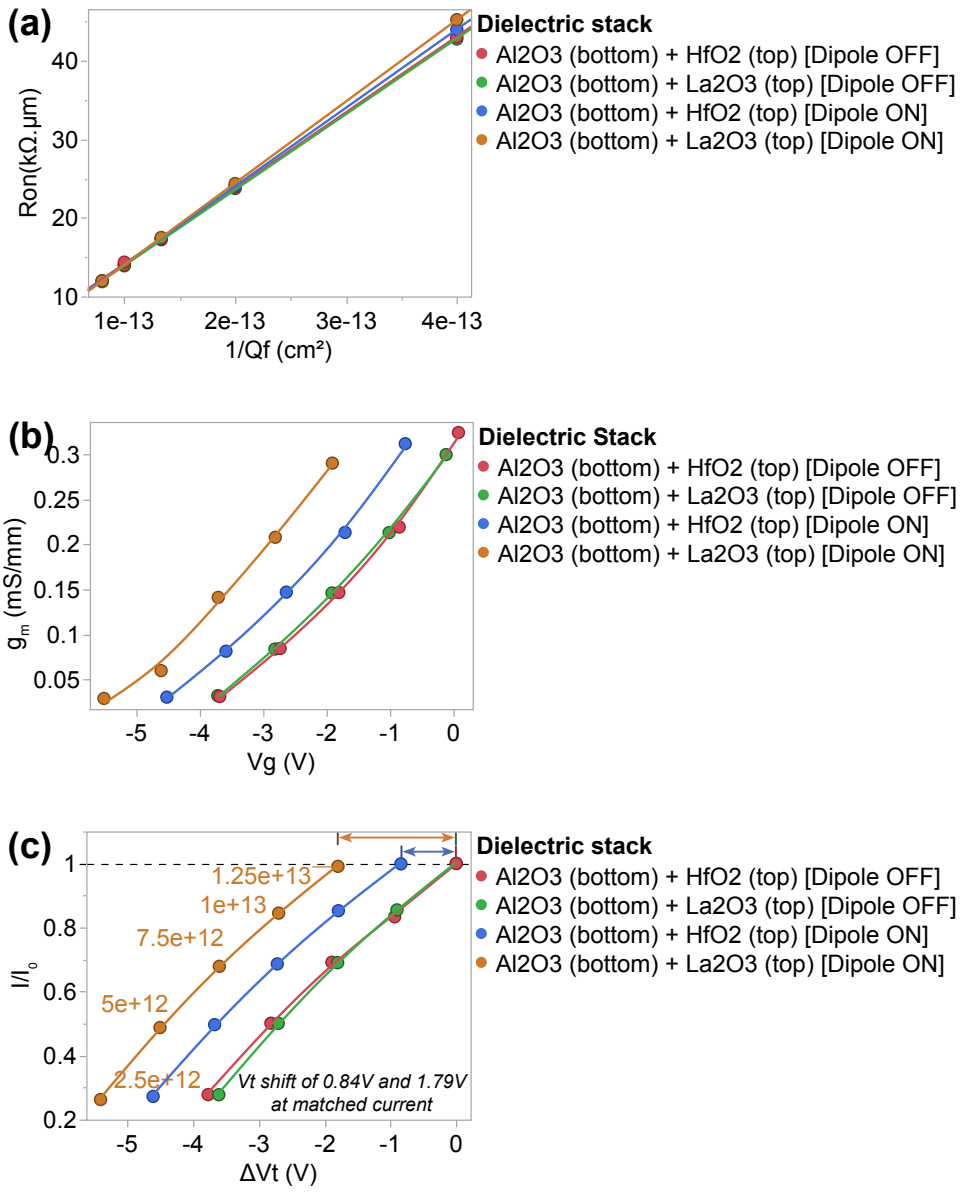


Fig. 7 **(a)** R_{on} vs $1/Q_f$ for both dipole stacks for Dipole ON and OFF **(b)** g_m at matched overdrive for different Q_f values for both dipole stacks for Dipole ON and OFF **(c)** I/I_0 vs ΔV_t for both dipole stacks for Dipole ON and OFF

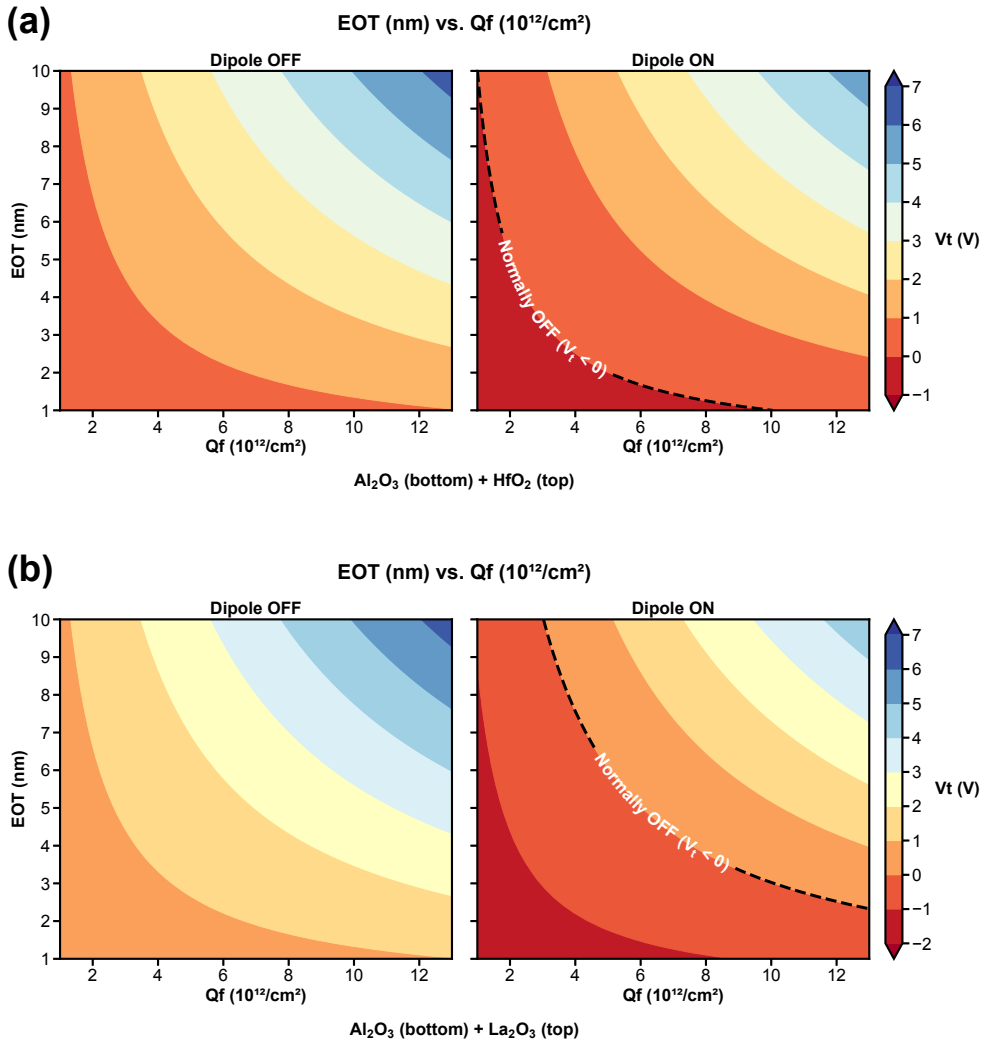


Fig. 8 Dipole V_t design window for **(a)** Al_2O_3 (bottom)/HfO_2 (top) **(b)** Al_2O_3 (bottom)/La_2O_3 (top), for Dipole ON vs Dipole OFF conditions